

PQDynamicISP: Dynamically Controlled Image Signal Processor for Any Image Sensors Pursuing Perceptual Quality

Masakazu Yoshimura¹, Junji Otsuka¹, and Takeshi Ohashi¹

Sony Group Corporation, Tokyo, Japan

{Masakazu.Yoshimura, Junji.Otsuka, Takeshi.A.Ohashi}@sony.com

Abstract. Full DNN-based image signal processors (ISPs) have been actively studied and have achieved superior image quality compared to conventional ISPs. In contrast to this trend, we propose a lightweight ISP that consists of simple conventional ISP functions but achieves high image quality by increasing expressiveness. Specifically, instead of tuning the parameters of the ISP, we propose to control them dynamically for each environment and even locally. As a result, state-of-the-art accuracy is achieved on various datasets, including other tasks like tone mapping and image enhancement, even though ours is lighter than DNN-based ISPs. Additionally, our method can process different image sensors with a single ISP through dynamic control, whereas conventional methods require training for each sensor.

Keywords: Image signal processor · image enhancement

1 Introduction

Image Signal Processors (ISPs) convert RAW images from image sensors into standard RGB (sRGB) images that appear natural and pleasing to the human eye. The pixel values in the RAW image are determined by the physical brightness and image sensor’s characteristics. Similarly, the human eye has its own response characteristics to light, adapting to dark or light environments and perceiving colors accurately regardless of ambient light color. Additionally, the relationship between physical brightness and perceived brightness is non-linear (approximately $y = x^{1/3}$) [54]. Therefore, ISPs need to cancel out the sensor characteristics and then mimic the human eye’s response in order to capture the landscape as the human actually perceives it. Furthermore, some flavoring (*e.g.*, making the sky bluer than it actually is) may be added [6].

Conventional ISPs address these challenges by creating and tuning individual functions, such as demosaicing to increase resolution while minimizing artifacts like false color and moire, color correction function to cancel out the sensor’s color filter characteristics, denoising to reduce sensor noise, gain adjustment to mimic the eye’s light/dark adaptation, white balance to mimic color adaptation, and gamma and tone mapping to mimic the human stimulus response. While

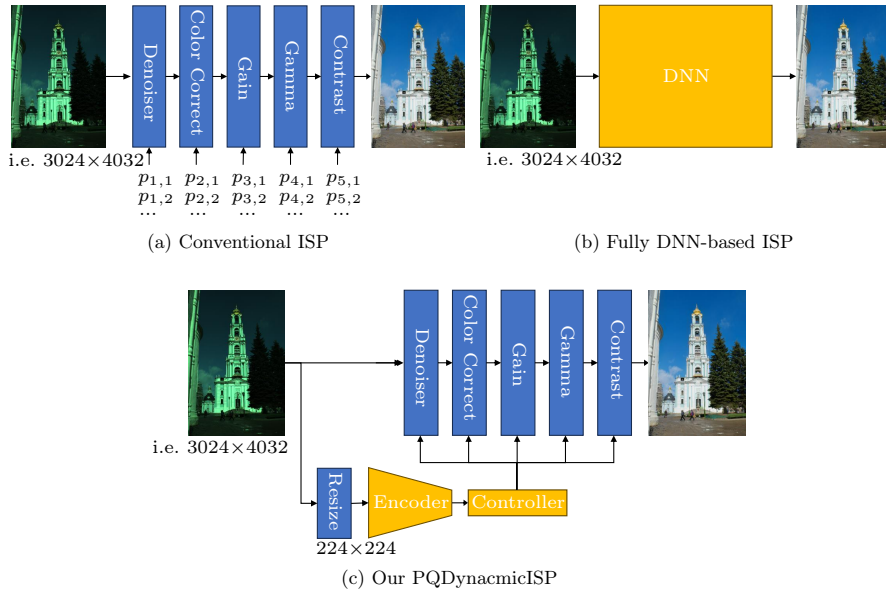


Fig. 1: (a) The conventional ISPs tune the parameters of classical ISP functions for each image sensor, while (b) the fully DNN-based ISPs train DNN for each image sensor. (c) Our method handles any sensors by controlling the parameters of classical ISP functions for each environment and each sensor, and even locally.

conventional ISPs are lightweight, they lack expressiveness and require significant time to tune for each image sensor [38].

As a result, there has been extensive research on full Deep Neural Network (DNN)-based ISPs [14, 20, 27, 29], which have demonstrated superior image quality. However, their computational costs are high because even smartphone cameras tend to require 12MP ($4032 \times 3024 \times 3$) resolution images, which is much higher resolution than the input of typical image recognition DNNs. Also, existing DNN ISPs are trained for each image sensor because their characteristics are very different.

While DNN ISPs have been actively studied for perceptual quality, in the field of image recognition, it has been proven that processing RAW images with a part of conventional ISP functions before feeding them into image recognition DNNs can improve recognition accuracy [22, 38, 44, 62]. We infer from this that the data distribution of RAW images is challenging to handle solely with DNNs. Additionally, several methods improve recognition accuracy even more by dynamically controlling the parameters of the classical ISP functions to make it easier for the recognition DNN to recognize [34, 45, 46, 61].

Therefore, we challenge the realization of a lightweight and high-quality ISP by dynamically controlling the parameters of conventional ISPs for perceptual image quality. For image recognition purposes, it is sufficient to control a portion of the ISP functions since downstream recognition DNNs have the ability to

process any data distributions to some extent. Even if the control fails, it is acceptable as long as the recognition DNN recognizes the image correctly [34, 61]. However, when it comes to the ISP for perceptual image quality, it is crucial to successfully address the cancellation of sensor characteristics, adaptation to human eye characteristics, and flavoring without failure. Another problem is that classical ISP functions have many local minima [55]. In this work, we propose training methods to tackle these challenges. Furthermore, to enhance performance, we make the ISP parameters controllable not only frame by frame but also locally. As a result, our work outperforms even large-scale NNs.

The mechanism of the dynamic ISP control has the potential to create a universal ISP that can handle various image sensors. It can predict sensor characteristics based on input images and automatically determine the appropriate parameters for each sensor and environment. We introduce a new task in which RAW images from various image sensors are processed without any distinctions. Our results demonstrate significant advantages over existing works. A single ISP that can be used across different image sensors would be highly beneficial, eliminating the need for data collection and tuning for each individual sensor.

In summary, the contributions of this work are:

- Dynamic control of classical ISP functions for image quality is proposed and achieves state-of-the-art image quality that surpasses large DNN ISPs.
- Our proposed method not only controls ISP parameters frame by frame but also locally, resulting in further improvements in accuracy.
- Training methods to deal with the local minima in the ISP are proposed.
- We newly define an universal ISP task and demonstrate that our method offers significant advantages over existing methods.
- Furthermore, we repurpose our ISP for tone mapping and enhancement tasks, showcasing its versatility.

2 Related Works

2.1 ISP

As mentioned above, ISPs have various roles, so in the early era, each function such as white balance [10, 56], denoiser [5, 13], and tone mapping [16, 21, 51], evolved as separate algorithms. Even now, improving each algorithm of white balance [4, 18], denoiser [31, 70], and tone mapping [31, 59, 60] using DNNs is an important research topic. On the other hand, research on end-to-end ISP parameter tuning has also emerged to improve perceptual image quality [25, 38, 43, 58] and downstream recognition accuracy [38, 39, 62].

In recent years, full DNN-based ISPs have been actively studied. PyNet [29] and AWWNet [14] propose high-quality DNN-based ISPs. More recently, many efforts have been made to develop practical lightweight DNN ISPs for smartphones and DSLR cameras [20, 27, 67].

However, ISPs have various roles, so the difficulty of replacing an ISP with a single DNN is becoming apparent. For example, CameraNet [32] shows significant improvement in image quality by splitting the ISP into two DNNs: an

image restoration DNN and a color manipulation DNN. Deep-FlexISP [33] won the NTIRE 2022 challenge [17] by further splitting it into three DNNs. In the following year, a method that carefully tunes classical ISP functions [69] won the NTIRE 2023 challenge [52], suggesting that classical ISP functions are still competitive depending on the quality and quantity of the dataset.

2.2 Dynamic Control and Local Parameter Tuning of ISP

Dynamic ISP control to improve downstream image recognition has started to emerge. Two works control a classical elaborate black box ISP [45, 46] for a frozen downstream detector. They also show potential for improving image quality in a toy task. K. Q. Dinh *et al.* [15] and DynamicISP [61] achieve significant accuracy improvement by controlling several simple differentiable ISP functions and optimizing the ISP and downstream model end-to-end. Several inverse ISP methods also control the parameters of inverse ISP functions [11, 40].

For the tone mapping task, which is part of the ISP task, many methods achieve high image quality by generating a 3D look-up table for each image [59, 60, 64]. These are also a type of dynamic ISP control, but the cost of practical use in small devices is high due to high memory consumption [12] and lack of backend implementations, such as ONNX Runtime [2] and TensorFlow Lite [3]. Therefore, in this study, we only control the parameters of simple functions.

In addition, local tone mapping, which tunes ISP parameters locally based on local luminance distribution, has improved visibility in HDR environments [21, 51]. Based on the local tone mapping idea, we propose a method to control ISP parameters not only frame by frame but also locally.

3 Methodology

As mentioned above, we propose dynamic ISP parameter control for perceptual image quality. The basic idea is based on DynamicISP [61], a method used for enhancing image recognition. We need to propose a new method because it requires finer control to achieve high image quality that feels natural to people, rather than just being able to distinguish what an object is. The proposed model structure and its training method are described below. The model structure can be divided into three main parts: the ISP, the lightweight encoder, and the controller that determines the ISP parameters, as shown in Fig. 1(c).

3.1 ISP

Conventional ISPs used in smartphones and SLR cameras are not as redundant as DNNs, but they are complex with many hyper-parameters. It was found that the computing speed is slow despite their FLOPs due to the lack of optimization in deep learning frameworks. Therefore, we propose an ISP that is as lightweight as possible, while having generality that can be used for various datasets. The proposed ISP consists of only five elements: denoiser I_{DN} , color correction I_{CC} ,

gain I_{GA} , tone mapping I_{TM} , and contrast stretcher I_{CS} . The input image X is sequentially processed by them like, $I_{CS}(I_{TM}(I_{GA}(I_{CC}(I_{DS}(X)))))$. We define the input and output range of the ISP as $[0, 1]$ in the following formulas.

Denoiser. While DynamicISP uses a simple Gaussian denoiser, DNN-based denoisers are powerful. In pursuit of perceptual quality, other filtering processes such as demosaicing, blur removal, and sharpening are also necessary, and a single DNN can encompass multiple filtering processes. Therefore, a DNN is used as a denoiser in this work. However, the computational cost of even a few-layer DNNs is enormous when processing high-resolution images.

Therefore, we propose a denoiser built with a tiny CNN, but some of the convolution kernels are dynamically generated to increase the expressive power as shown in Fig. 2. Specifically, a depth-wise convolution kernel is generated for each image: $I_{Dy}(X) = Conv(P_{filter}, X)$, where P_{filter} is a depth-wise convolution kernel of $C_{in} \times 1 \times k \times k$ size. If the local ISP control proposed later is used, it becomes a depth-wise dynamic filter of $H \times W \times C_{in} \times 1 \times k \times k$ size. Conventional dynamic filter methods generate filters from the previous intermediate features [49, 68], so they are necessary to encode high-resolution features. However, our method uses the controller described later to generate filters, which successfully reduces the computational cost.

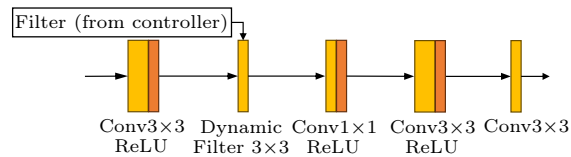


Fig. 2: The proposed light weight denoiser.

Color Correction Including White Balance. The general color correction matrix cancels the color filter characteristic of the sensor and is a fixed 3×3 matrix. Our method, on the other hand, controls nine parameters of a 3×3 matrix P_{CC} in the following function; $I_{CC}(X) = XP_{CC}$. In usual ISPs, white balance is also used as a separate module from color correction to imitate the human eye’s color adaptation characteristics. However, to reduce the computational cost, we make our color correction function simultaneously cancel the color filter characteristics and imitate the color adaptation.

Gain. Our gain function is based on DynamicISP’s implementation, which amplifies image values while avoiding overflow from $[0, 1]$ without clipping. We improve the expressive power without increasing the computational cost by using different parameters for each color channel, $c = \{r, g, b\}$, as follows;

$$I_{GA}(X_c) = \begin{cases} \frac{1-p_{h,c}}{1-p_{w,c}} X_c & (\text{if } x_c < p_{x,c}(1-p_{w,c}), x_c \in X_c) \\ \frac{1-p_{h,c}}{1-p_{w,c}} X_c + \frac{p_{h,c}-p_{w,c}}{1-p_{w,c}} & (\text{if } p_{x,c}(1-p_{w,c}) + p_{w,c} < x_c) \\ \frac{p_{h,c}}{p_{w,c}} (X_c - p_{x,c}(1-p_{w,c})) + p_{x,c}(1-p_{h,c}) & (\text{otherwise}) \end{cases}, \quad (1)$$

where X_c is each channel array of X . We further improve the function by decorating $p_{x,c}$ as $p_{x,c} = 10^{p'_{x,c}}$ to control dark areas more precisely, as the dark value is stretched in the subsequent module of tone mapping.

Tone Mapping. We follow the parameterization of the previous gamma tone mapping [38, 61, 62] and further parameterize it by using different parameters for each color channel as follows;

$$I_{TM}(X_c) = X_c \frac{\frac{1}{p_{\gamma 1,c}} \cdot \frac{1-(1-p_{\gamma 2,c})X_c^{\frac{1}{p_{\gamma 1,c}}}}{1-(1-p_{\gamma 2,c})p_{k,c}^{\frac{1}{p_{\gamma 1,c}}}}}{1-(1-p_{\gamma 2,c})p_{k,c}^{\frac{1}{p_{\gamma 1,c}}}}. \quad (2)$$

Contrast Stretcher. As the recognizer can process values other than $[0, 1]$, DynamicISP simply uses the linear function $Y = p_a X + p_b$. However, for perceptual image quality, it is necessary to keep the value within $[0, 1]$. So eq. 1 is used again but, as it is after tone mapping, the further decoration is not used.

Inverse Tone Mapping. We attempt to apply our work not only to the ISP task but also to the enhancement task, which converts sRGB images to clean sRGB images. In this case, an inverse tone mapping function is added at the beginning of our ISP to convert the original sRGB to linear sRGB. We construct the following function to be similar to the inverse function of eq. 2:

$$I_{IT}(X_c) = X_c \frac{p_{\gamma 3,c} \cdot \frac{1+p_{\gamma 4,c}(X_c+1)^{p_{\gamma 3,c}}}{1+p_{\gamma 4,c}(p_{k2,c}+1)^{p_{\gamma 3,c}}}}{1+p_{\gamma 4,c}(p_{k2,c}+1)^{p_{\gamma 3,c}}}. \quad (3)$$

3.2 Encoder

In DynamicISP, an intermediate feature of a recognizer is used as an information source to determine the ISP parameters. However, ISP control for perceptual image quality requires an image encoder to obtain the feature and determine the ISP parameters. Therefore, a lightweight encoder is proposed as shown in Fig. 3(a). First, any resolution of inputs is resized to a fixed resolution in order to reduce computational costs. Since the SYENet block achieved high performance in image restoration with only a few layers of CNNs [20], we assumed that the SYENet block could generate a good feature with a few layers. However, unlike when using the SYENet block for image restoration, it was found that the training loss exploded when using it as a feature extractor, as there are fewer constraints on the output of the encoder. Therefore, layer normalization is added as shown in Fig. 3(b). In addition, stride convolution is introduced to the first layer of each block to reduce computational costs significantly.

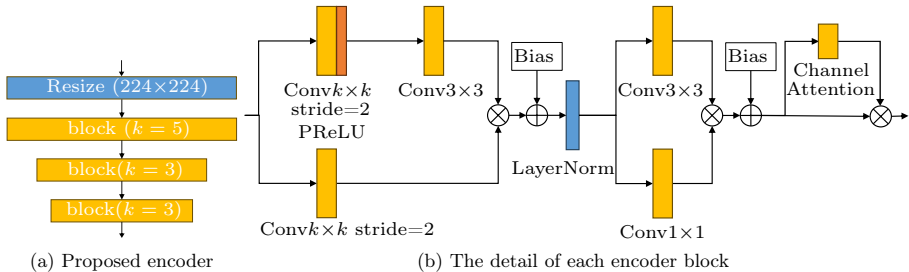


Fig. 3: The proposed (a) light weight encoder consists of three (b) blocks modified from the SYENet block [20].

3.3 Controller

Our controller controls the ISP parameters based on the feature from the encoder. We propose two controllers: a lightweight global controller and a more precise local controller.

Global Control. In the global control, the ISP parameters are controlled per image. Therefore, global average pooling is applied to the encoder’s output to create global latent variable V_0 , and the parameters are determined with a fully connected layer $f_{full,l}$ as follows:

$$P_l = f_{dec,l}(V_{l-1}) = f_{act,l}(\hat{P}_l + f_{full,l}(V_{l-1})), \tag{4}$$

where V_{l-1} is the latent variable to decide ISP parameters P_l in the l -th ISP layer, and \hat{P}_l are learnable parameters. Following DynamicISP, we define $f_{act,l}$ as

$$f_{act,l}(x) = (P_{l,max} - P_{l,min}) \cdot sigmoid(x) + P_{l,min}, \tag{5}$$

to control parameters within $(P_{l,min}, P_{l,max})$. We update the latent variable considering what ISP parameters are used in each layer by $V_l = f_{up,l}(V_{l-1}, P_l)$ the samely with DynamicISP but we use proposed group-wise sigmoid cross-attention as $f_{up,l}$ to achieve precise control. It is different from usual cross-attention [47] in six points as shown in Algorithm 1; (1) linear layers are only used for generating the key, (2) the content input (P_l) is not used as the source of the value, (3) sigmoid is used instead of softmax for the attention, (4) the last matrix multiplication with the value is replaced with a Hadamard product, (5) the last feed forward network is not used, and (6) a virtual sequential length is introduced. Unlike vision transformers, the sequential length of the input is one. So, we group the channel dimension of the latent variable V_{l-1} with the virtual sequential length and attend within the groups. The motivation for the proposal is as follows. If normal cross-attention is used, the distribution of the query (V_{l-1}) is mixed according to the key (P_l) and value (P_l). However, in the current problem set-up, the sources of the key (P_l) and value (P_l) are a few parameters, and they don’t have enough information to mix the high-dimensional

Algorithm 1: Group-wise Sigmoid Cross-Attention

```

def __init__(C, Num_param, vertical_seq):
    emb_dim = C/vertical_seq
    linears = Sequential(Linear(), ReLU(), Linear(c_out=emb_dim**2))
    scale = emb_dim ** -0.5
def forward( $V_{l-1}$ ,  $P_l$ ): # [B,C], [B, (l-th ISP layer's) Num_param]
    q =  $V_{l-1}$ .reshape(B, vertical_seq, emb_dim)
    k = linears(( $P_l - P_{l,min}$ ) / ( $P_{l,max} - P_{l,min}$ ))
    k = k.reshape(B, emb_dim, emb_dim)
    v =  $V_{l-1}$ 
    attn = 5 * sigmoid(q@k * scale).view(B, -1)
     $V_l$  = v*attn
return  $V_l$ 

```

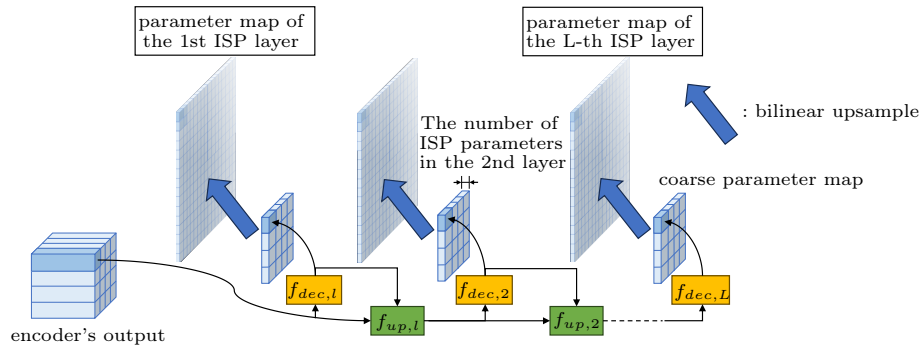


Fig. 4: The proposed local controller. In practical implementation, we don't iterate per region but compute at once using point-wise convolutions within $f_{dec,l}$ and $f_{up,l}$.

V_{l-1} appropriately. Therefore, not to corrupt the distribution of V_{l-1} , our method determines how much each value of V_{l-1} should be changed considering P_l and V_{l-1} of the same group, and just multiplies to V_{l-1} using a simple Hadamard product.

Local Control. In local control, the ISP parameters are controlled on a pixel-by-pixel basis in addition to an image-by-image basis. However, if the control is completely per-pixel, the computational cost of generating ISP parameters is high and the accuracy is not good due to too many degrees of freedom. Therefore, the ISP parameters are generated at the coarse resolution of the encoder output, which is then expanded to the original image size by bilinear upsampling. In other words, the global average pooling for global control is removed, the parameters are generated for each region of the encoder's output resolution in the same way as global control, and finally bilinear upsampling is applied as shown in Fig. 4.

Algorithm 2: Automatic Tuning of Parameter Search Spaces

```

 $P_{min}, P_{max}$  = init(initialize with enough large search spaces)
for s in range(S) # S: total training stages
    losses = array([T])
    params = array([T,N,D]) # N: #ISP params, D: #training data
    for t in range(T) # train T times with different random seeds
        l_fs, p_fs = train(model)
        losses[t] = mean(l_fs) # losses in the final epoch
        params[t, :, :] = p_fs # used ISP param. in the final epoch
     $t_{best}$  = losses.argmaxin()
    # update search space
     $P_{min}$  = r * params[ $t_{best}$ ].min(dim=-1) + (1-r) *  $P_{min}$ 
     $P_{max}$  = r * params[ $t_{best}$ ].max(dim=-1) + (1-r) *  $P_{max}$ 

```

3.4 Training Methods

Automatic Tuning of Parameter Search Spaces. As mentioned earlier, conventional ISPs are known to have many local minima [55], and in fact, our work also suffers from them. Specifically, as described in Appendix, completely different ISP parameters were chosen when changing the initial random seed, resulting in a slightly different accuracy. To solve this problem, we propose an *automatic tuning of parameter search spaces*. The idea is to create search spaces that do not contain local minima by making good use of the fact that our ISP functions are white-box, unlike typical DNNs. Specifically, local minima are excluded by appropriately narrowing the parameter search spaces ($P_{l,min}, P_{l,max}$). The algorithm is shown in Algorithm 2.

In the first training stage, the search spaces of parameters are set sufficiently wide, and the model is trained T times with different initial seeds. Then, we assume that the model with the best average loss value in the final epoch is the model that falls into the best local minima. We monitor the ISP parameters used by the best model during the final epoch, and update the parameter search spaces. By repeating this operation several times, search spaces excluding local minima as much as possible is obtained. Our ISP has a small number of parameters, so the loss value is not affected by overfitting, and the algorithm works well. Although the algorithm needs multiple times of training, the training cost is lower than other methods because the model itself is lightweight and the convergence is quick as described below.

Denoisier as Denoisier. We propose a training method for the case where DNN denoisier is used. As shown in the experiments, in tasks where denoisier is not required, the proposed method outperforms even large-scale DNN-based ISPs in terms of accuracy. From this, it can be inferred that the DNN is inferior to the proposed ISP control for color mapping. Therefore, when adding a DNN as a denoisier, we make the DNN perform only denoising. First, our model is trained with *automatic tuning of parameter search spaces* while removing the denoisier.

It allows our model to learn to map the color outside of the denoiser. Then, we add the denoiser and freeze the non-denoiser parts. This allows the denoiser to learn to perform only denoising. Finally, the whole model is finetuned. The final finetuning improves the image quality a little because the average luminance value can be changed due to noise removal and subsequent non-linear processing.

Local L1 Loss. In addition to the aforementioned *denoiser as denoiser*, the following loss function is further added to restrict the denoiser from changing color:

$$L_{LocalL1}(X) = L_1(AvgPool(I_{DN}(X)), AvgPool(X)),$$

where *AvgPool* is the average pooling with kernel size k_a and stride s_a .

4 Experiments

4.1 Datasets

The effectiveness of the proposed method is verified on various tasks and datasets. We evaluate on four tasks: the newly defined **universal ISP task**, where RAW images from any image sensors with unknown sensor characteristics need to be processed; the **normal ISP task**, where RAW images from a specific sensor are processed; the **tone mapping task**, where standardized CIE XYZ images after canceling sensor characteristics and environment light are converted into sRGB; and the **enhancement task**, where original sRGB images are converted into high-quality sRGB images.

The universal ISP task is evaluated on the MIT-Adobe FiveK dataset [6]. The dataset consists of RAW images from 17 different image sensors paired with sRGB images from hardware ISPs and manually retouched ground truth sRGB images. We follow the convention on FiveK in the enhancement task [9, 60, 64]; the sRGB images retouched by expert C are used as the ground truth, and 500 out of 5,000 images are defined as the test data. Since their Bayer patterns are diverse per each sensor, we demosaic them as a preprocessing and resize them isotropically into 480P size, whose shorter edge length is 480. For the normal ISP task, the MAI21 dataset [26] is used. In this dataset, the RAW images from a smartphone sensor are inputs, and sRGB images from a high-quality SLR camera are the ground truth. Since the MAI2022 challenge [28], the last competition on the MAI21 dataset, is finished and only the training data is accessible, 10% of the training data is defined as the test data. As the images with close image IDs are patches cut from the same image, the last 10% of the image IDs are used as test data without shuffling. For the tone mapping task, the FiveK and HDR+ [23] datasets are used. HDR+ is a burst photography dataset. Following previous works [64, 65], the intermediate 480P size 16-bit results after HDR composition are used as the input, and JPEG images from a manually tuned HDR imaging pipeline are used as the ground truth. The 247 out of 922 images are defined as the test data. This dataset requires not only tone mapping but also enhancement because some images are very dark. For the enhancement task, the widely used FiveK dataset is used.

Table 1: Evaluation on FiveK dataset. The faster runtime on TensorRT or PyTorch is reported. Improved runtimes with original CUDA kernels are written in (). More details of runtime are reported in the Appendix. The upper rows are general image restoration models for small images, and the lower rows are specialized real-time models.

	universal ISP		tone mapping		enhancement		runtime [ms]	
	PSNR	SSIM	PSNR	SSIM	PSNR	SSIM	480P	4K
Restormer [63]					24.13			
NAFNet-small [8]	22.53	0.891	24.73	0.920	24.52	0.912	54.75	1428.60
Retinexformer [7]					24.94			
UPE [57]			21.56	0.837	21.88	0.853	4.27	56.88
MicroISP [27]	21.64	0.885	24.07	0.909	23.92	0.909	5.11	114.13
HDRNet [19]			24.52	0.915	24.66	0.915	3.49	56.07
3D LUT [64]			25.06	0.920	25.21	0.922	- (1.02)	- (1.14)
CSRNet [24]			25.19	0.921	25.17	0.921	3.09	77.10
SYENet [20]	22.24	0.889	25.19	0.922	25.04	0.916	1.26	31.53
RSFNet [41]					25.49	0.924	9.98	
AdaInt [59]			25.28	0.925	25.49	0.926	- (1.29)	- (1.59)
SepLUT [60]	22.82	0.891	25.43	0.922	25.47	0.921	6.18 (1.10)	128.5 (1.20)
F. Zhang <i>et al.</i> [65]			25.53	0.907				
ours (global)	22.99	0.901	25.35	0.928	24.80	0.918	1.00	4.49
ours (local)	23.59	0.911	25.72	0.933	25.53	0.928	1.14	11.61

4.2 Implementation Details

We use almost the same experimental settings for all tasks and datasets. Our model is trained with the AdamW optimizer [36] from randomly initialized weights using a cosine annealing learning rate schedule [35], whose maximum and minimum learning rates are $1e-4$ and $1e-7$, with a linear warmup for the first 1,000 iterations. Random flip, rotation, and crop are applied to augment the training data except for MAI21. On MAI21, no augmentations are applied because the input is in Bayer pattern. Based on the dataset sizes, we train 100 epochs on FiveK, 30 epochs on MAI21, and 600 epochs on HDR+. The mini-batch size is 16. Although the 480P size of the FiveK dataset contains various image sizes such as 480×720 , 720×480 , 480×640 , they are resized to 640×480 to achieve fast mini-batch training. During inference, original 480P size images are used to evaluate. The denoiser is used only for MAI21, a dataset that requires denoising. Its middle channel size is set as 12. The loss function is a combination of mean square error loss and perceptual loss [30] with trained VGG16 [53]: $L = L_{MSE} + 0.1L_{VGG}$. When adding the denoiser, the proposed *local L1 loss* is added with a strength of 0.01. For more details, please refer to the Appendix.

4.3 Evaluation on FiveK Dataset

The results on the three tasks are shown in Table 1. All tasks of NAFNet [8], MicroISP [27], and SYENet [60], and the universal ISP task of SepLUT [60] are evaluated by us, and others are taken from other papers. These models have slower convergence compared to ours, so we trained them for 500 epochs following Retinexformer [7] to ensure fairness. The runtime is measured on a

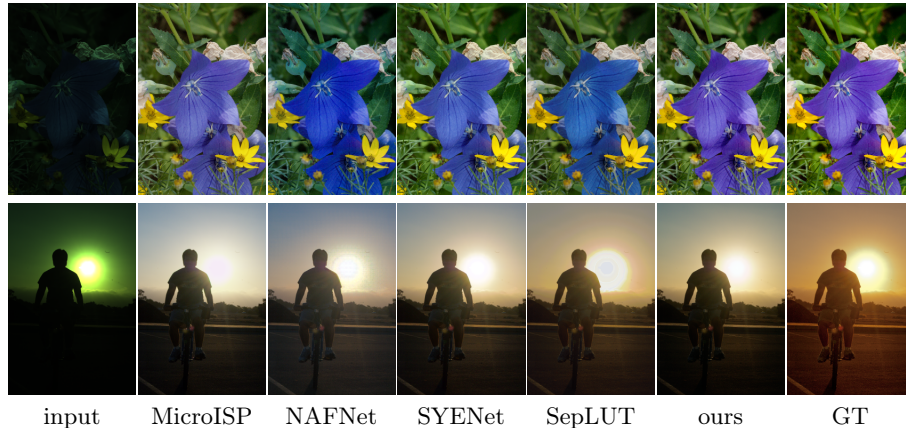


Fig. 5: Visualization of the universal ISP task on FiveK [6]. Our method estimates the true color well without artefacts. (Please zoom in.)

V100 GPU using two implementations, Pytorch [42] and TensorRT [1], and the faster one with float32 precision is described. For more details, please refer to the Appendix.

Firstly, the universal ISP task is the most challenging, resulting in low accuracy for all methods. However, our method significantly outperforms existing methods, demonstrating its ability to cancel sensor-specific characteristics through dynamic ISP control. DNN-based ISPs with excessive degrees of freedom and SepLUT with more degrees of freedom than our method do not learn well as shown Fig. 5. Secondly, our method achieves the highest accuracy in the tone mapping task among all tasks and methods. Since our method is designed as an ISP, it performs exceptionally well in tone mapping, which is a partial task of ISPs. Although our accuracy for the enhancement task is not as good as that of the tone mapping task, it is more accurate than existing methods. Further improvement can be made by enhancing the inverse tone mapping function.

Despite achieving state-of-the-art accuracy, the runtime of our method is significantly faster than existing methods. Look-up table-based methods greatly improve runtime on high-resolution images by implementing a CUDA kernel [59, 60, 64, 65]. Our method can also be improved by implementing a CUDA kernel. As memory transfer costs are high for high-resolution images, combining the entire ISP functions into a single CUDA kernel can lead to a significant speed up. However, this is a trade-off with versatility, as devices like smartphones do not support CUDA.

How the proposed components contribute to the performance is described in Table 2(a). *Automatic tuning of parameter search spaces* partially solves the local minima problem and improves the accuracy. The proposed encoder also succeeds in generating better features despite the size. Furthermore, the *group-wise sigmoid cross-attention* used as f_{up} improves the accuracy over the normal cross-attention as intended.

Table 2: (a) Ablation studies on FiveK and (b) the benchmark on HDR+ in the tone mapping task. In the ablation study, the proposed *automatic tuning of parameter search spaces* (ATPS), encoder, and f_{up} in the controller are evaluated. The more detailed ablation studies are reported in the Appendix.

(a) ablation studies on FiveK					(b) benchmark on HDR+		
ATPS	encoder block	f_{up}	PSNR	runtime 4K		PSNR	SSIM
			25.62	11.61	CSRNet [24]	23.72	0.864
	✓	✓	25.30	12.28	3D LUT [64]	23.54	0.885
✓	[8]	✓	NaN		HDRNet [19]	24.14	0.845
✓	[20]	✓	25.64	11.65	DeepLPF [37]	25.73	0.902
✓	✓	cross-attn	25.63	11.59	CLUT-Net [66]	26.05	0.892
✓	✓	[61]	25.72	11.61	F. Zhang <i>et al.</i> [65]	26.62	0.907
✓	✓	✓			ours (global)	22.26	0.869
					ours (local)	26.72	0.927

4.4 Evaluation of the Tone Mapping Task Including Low-light Enhancement on HDR+ Dataset

Since HDR+ contains more HDR and darker scenes than the FiveK tone mapping task, the ISP parameters need to be controlled more dynamically. Our method succeeds in controlling them appropriately and achieves state-of-the-art accuracy, as shown in Table 2(b). There is a significant advantage of local control over global control in HDR+ compared to FiveK. This is probably because the input and ground truth of HDR+ are created from different source data, *i.e.* several burst RAW images are combined with different proportions, which requires non-global mapping. On the other hand, the ground truth of FiveK is created by hand-tuning global parameters, so in principle, global control alone is sufficient. However, the degree of freedom of the ISP function is limited, so local control may have improved the accuracy somewhat. To maximize the benefits of the proposed local control, it is necessary to prepare datasets like HDR+ or more locally tuned datasets.

4.5 Evaluation of the Normal ISP Task on MAI21 Dataset

On MAI21, our ISP including the proposed denoiser is evaluated. MicroISP and SYENet are trained for 200 epochs instead of 30 epochs, following the original setup of SYENet. As shown in Table 3(a), our work also outperforms in tasks that require a denoiser. Unlike the results on FiveK, our method with local control is slower than SYENet. This is because our method performs the demosaicing included in our denoiser first, and the high-resolution image has to be processed in the remaining ISP functions. It can be solved if the demosaicing is done at the end, but it will become a trade-off between accuracy and speed. Furthermore, as noted in the appendix, the number of operations in our ISP is significantly less than that of CNNs and look-up tables and is only slow because small calculations are spread out. If an optimized implementation per backends such as combining ISP functions into a single CUDA, similar to 3D LUT [64] and SepLUT [60], the speed would increase dramatically.

Next, we discuss the additional DNN denoiser in our ISP. First, as shown in 3(b), controlling the dynamic filter with the proposed local control significantly improves the accuracy. Although it increases the runtime, the accuracy is better than using SYENet as the denoiser of our ISP. Furthermore, the increased runtime is due to our implementation using an unfold function and matrix multiplication, which is convertible to various backends. Our dynamic filter needs less computation than DDF [68], which is faster than standard convolution with an optimal implementation. Next, the accuracy deteriorates when the denoiser is trained at the same time. This is because the DNN denoiser performs part of the tone mapping, even though our simple ISP functions are superior to DNNs in terms of tone mapping, as shown in the evaluation on FiveK. The proposed *denoiser as denoiser* and *local L1 loss* improve the accuracy by letting the DNN denoiser only denoise.

Table 3: Evaluation on MAI21 in the normal ISP task. (a) The top four methods in the MAI2022 ISP challenge report [28] are listed. (b) The ablation studies regarding the denoiser in our ISP are conducted, including the proposed training methods of *denoiser as denoiser* (DasD) and *local L1 loss* (LocalL1).

	(a) benchmark						(b) ablation studies				
	official test score	PSNR	our split PSNR	SSIM	runtime (full HD) mobile	V100	type	DasD	LocalL1	PSNR	runtime
MicroISP [27]	9.25	23.87	23.00	0.799	23.1	8.28	none			24.18	3.26
ENERZAi	10.27	23.80			18.9		SYENet [20]			24.08	6.03
MiAlgo	14.87	23.30			6.8		SYENet [20]	✓	✓	24.59	6.03
SYENet [20]	21.24	23.96	24.32	0.860	11.4	2.39	wo dyFilter	✓	✓	24.47	4.38
ours (global)			23.67	0.835		2.76	w/ dyFilter			24.07	6.64
ours (local)			24.63	0.864		6.64	w/ dyFilter	✓	✓	24.61	6.64
							w/ dyFilter	✓	✓	24.63	6.64

5 Conclusion

This study proposes a new type of ISP for perceptual image quality that consists of very simple ISP functions, but the parameters are dynamically controlled to achieve high image quality. Unlike ISPs for image recognition, ISPs for perceptual quality require a great deal of processing to be done accurately. Our work achieves this by combining the proposed ISP functions, encoder, controller, and training method. Additionally, although not sophisticated, our work also performs well in the enhancement task by adding an inverse tone mapping function, demonstrating its versatility. Our work, which combines state-of-the-art lightness and state-of-the-art accuracy, will be useful in various situations, from applications in edge devices to operating in the cloud. Furthermore, the fact that it outperforms large-scale DNNs in terms of accuracy raises questions about the color-mapping capabilities of DNNs and may contribute to the future improvement of DNNs.

Appendix of “PQDynamicISP: Dynamically Controlled Image Signal Processor for Any Image Sensors Pursuing Perceptual Quality”

A More Implementation Details

Most of the implementation details are written in Section 4.2. More implementation details are given below.

The output channel size of each block of the encoder is set to 24, 48, and 96. The latent variable V_l in the controller is set to 256 for global control, as it is computationally inexpensive, and to 96 for local control. The kernel size k_a and stride s_a of the *local L1 loss* is set to 16 and 8. In the *automatic tuning of parameter search spaces*, two stages of training are performed, with five and four scratch training in each stage. Since the sigmoid function used for constraining search spaces in eq. 5 vanishes the gradient of the edge of the domain, it was observed that the accuracy deteriorates if the search spaces are too narrow. So, we set $r = 0.7$ in the Algorithm 2.

PSNR and SSIM are used as metrics. PSNR is calculated at the original resolution for all the datasets. On the other hand, SSIM is calculated differently per dataset following previous works. For the FiveK dataset, we calculate the SSIM after applying a low-pass filter and subsampling to 256×256 size following previous works [59,60,64]. For the HDR+ dataset, our table is mainly based on F. Zhang *et al.* [65], and they seem to calculate the SSIM at the original resolution. So we calculate it at the original resolution. For the MAI21 dataset, we calculate it at the original resolution because the original images are 256×256 patches.

B Ablation Studies on Local Control

The optimal resolution of the local control is investigated in addition to the effectiveness of adding decoder blocks in the encoder. We use a pixel shuffle [50] in our decoder block to upsample. As shown in Table 4, local control at a resolution of 28×28 is optimal, and when we try to control more finely, it becomes unstable and the accuracy deteriorates. It can also be seen that the accuracy is higher when no decoder blocks are used. This may be because the global features are well obtained by the attention in the encoder blocks, and the accuracy deteriorates as more global information is added by the decoder blocks. Although it could be improved by introducing skipping connections similar to Unet [48], we only use encoder blocks to save computational cost.

Table 4: Ablation studies on the optimal resolution of the local control and additional decoder blocks. The numbers in [] means the number of blocks in each encoder/decoder stage. The ablation study is conducted for the tone mapping task on FiveK dataset [6].

encoder architecture		controller's resolution	PSNR
encoder blocks	decoder blocks		
[1, 1]		56×56	25.60
[1, 1, 1, 1]	[1, 1]	56×56	25.47
[1, 1, 1]		28×28	25.72
[1, 1, 1, 1]	[1]	28×28	25.57
[1, 1, 1, 1]		14×14	25.44

C Local Minima in the ISP

In this section, how much the ISP parameters are controlled and how local minima exist in the ISP are discussed using Fig. 6. It shows the distributions of ISP parameters used by two models trained with different seeding. First, both models successfully control parameters, and that’s why our model achieves high accuracy with simple ISP functions. Second, although the accuracies of the two models are similar, the used ISP parameters are different. Similar accuracies with different parameters indicate that there are local minima. Furthermore, you can see that some local minima are quite far from each other which can not be overcome by devising an optimizer. So, it is preferable to train multiple times and choose a model that reaches better local minima by using *automatic tuning of parameter search*.

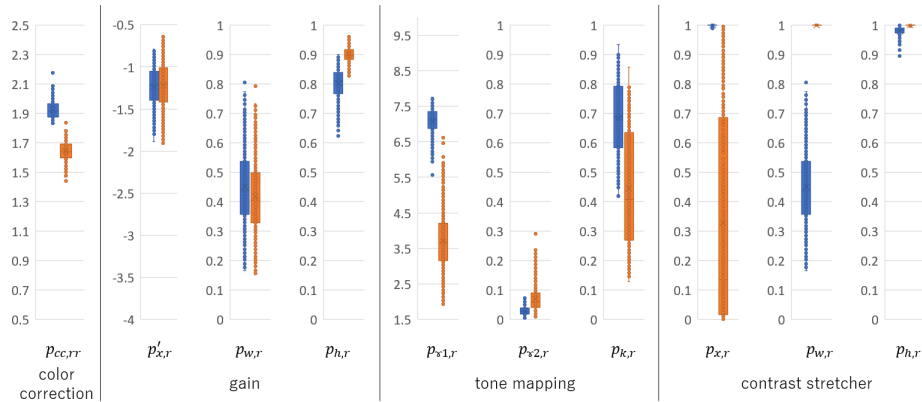


Fig. 6: For part of ISP parameters, the distributions of used parameters during test time are shown. The parameters used by two models with similar accuracy are plotted as blue (PSNR 26.2) and orange (PSNR 26.4). The existence of local minima is supported by the fact that they use different parameters but with almost identical accuracy.

Table 5: The detail of the runtime on two backends.

	Pytorch runtime [ms]		TensorRT runtime [ms]	
	480P	4K	480P	4K
NAFNet-small [8]	54.86	1428.60	54.75	OOM
MicroISP [27]	12.89	270.30	5.11	114.13
SYENet [20]	6.85	166.70	1.26	31.53
SepLUT [60]	6.18	128.5	31.1	804.60
ours (global)	6.98	107.9	1.00	4.49
ours (local)	11.20	172.00	1.14	11.61

D Details of Runtime

The faster runtime on TensorRT [1] or PyTorch [42] is reported in Table 1 of the main paper. Here, we report the details. As shown in Table 5, by converting from PyTorch models to TensorRT models, a significant speed improvement is observed for our model over other models. There are two possible reasons for this. One is that although the FLOPS of our controller is small thanks to the very small resolution, the number of functions in the controller is large. Pytorch implementation calls a lot of Python interfaces, which are time-consuming. By converting to TensorRT, the cost is reduced. In addition, in the ISP functions, although the FLOPS is less than one layer of convolution, simple operations such as quadrature operations are used a lot. In this case, because the images are high-resolution images, the memory transfer costs between functions are considered to be the reason for the slowdown. The speed could be further improved by combining the ISPs into a single kernel as described in the main paper. In fact, SepLUT [60] improves the speed from 51.19 ms to 1.20 ms by creating a single CUDA kernel. While SepLUT uses a 1D look-up table with 17 grids and a 3D look-up table with $17 \times 17 \times 3$ grids, our gain and contrast stretcher can be represented by a 1D look-up table with four grids.

E More Qualitative Comparison

Visual comparisons on the universal ISP task, tone mapping task, and enhancement task with FiveK dataset [6] are shown in Fig. 7. Also, the normal ISP task on MAI21 dataset and the tone mapping task on HDR+ dataset are shown in Fig. 8 and Fig. 9. Fig. 8 shows that our denoiser is working properly, not only denoising but also working for higher resolution. Although the accuracy of the denoiser looks not as good as that of recent large-scale DNNs, it works well considering the light weight. Fig. 8 shows the difference between the proposed global and local control. It can be seen that the local control is able to achieve vivid colors in high dynamic range (HDR) scenes, although whether the environment is bright or dark does not make much difference in accuracy.

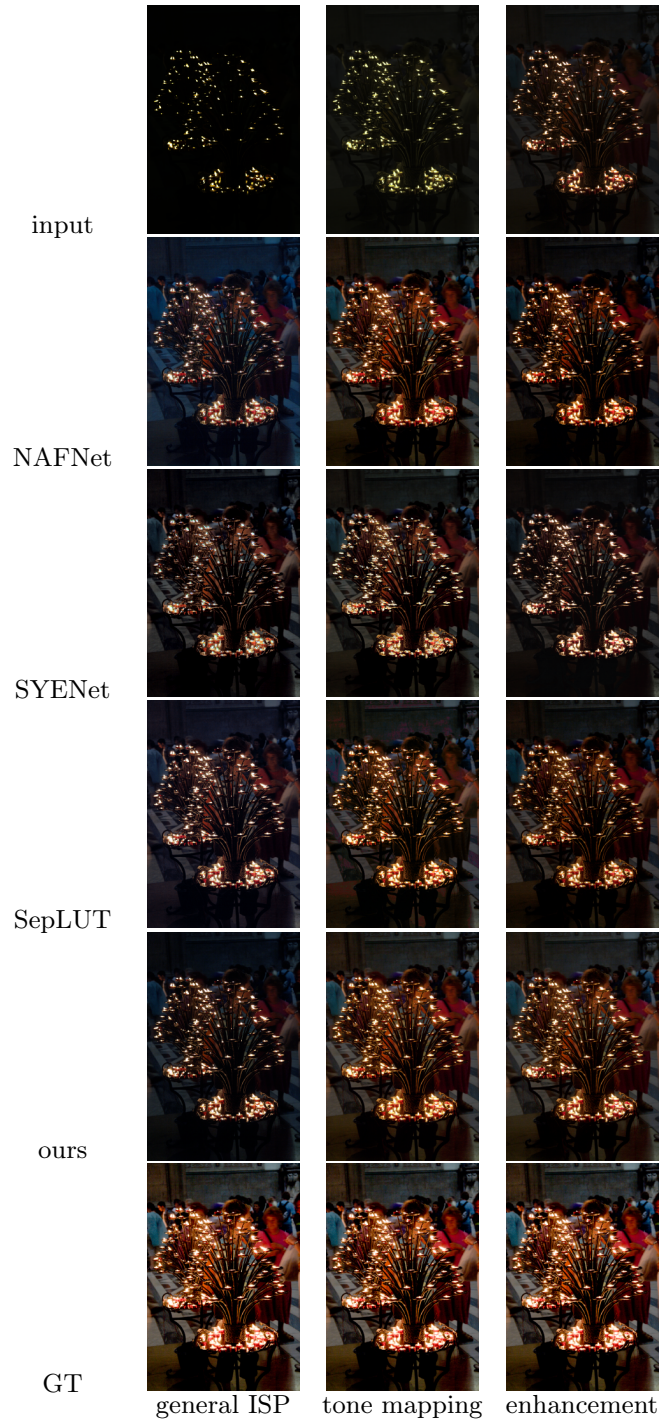


Fig. 7: Visual comparisons on FiveK [6].

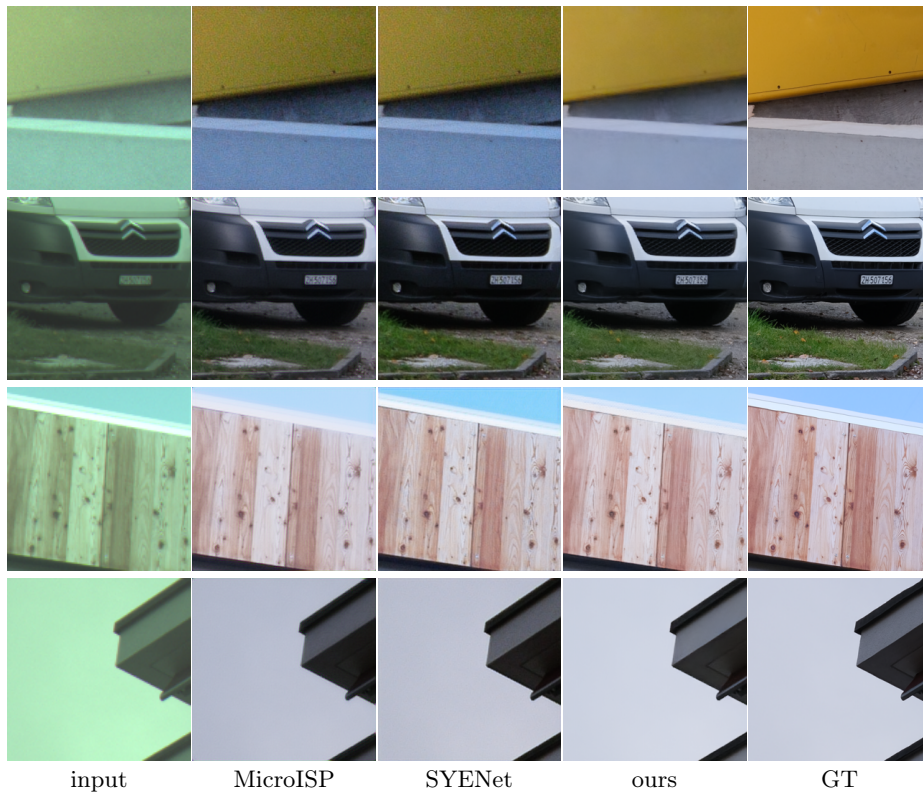


Fig. 8: Visual comparisons on MAI21 dataset [26]. The input RAW images are from a smartphone sensor, and the ground truth sRGB images are from a high-end DSLR camera. For visualization, we apply gain and gamma on the input RAW images.

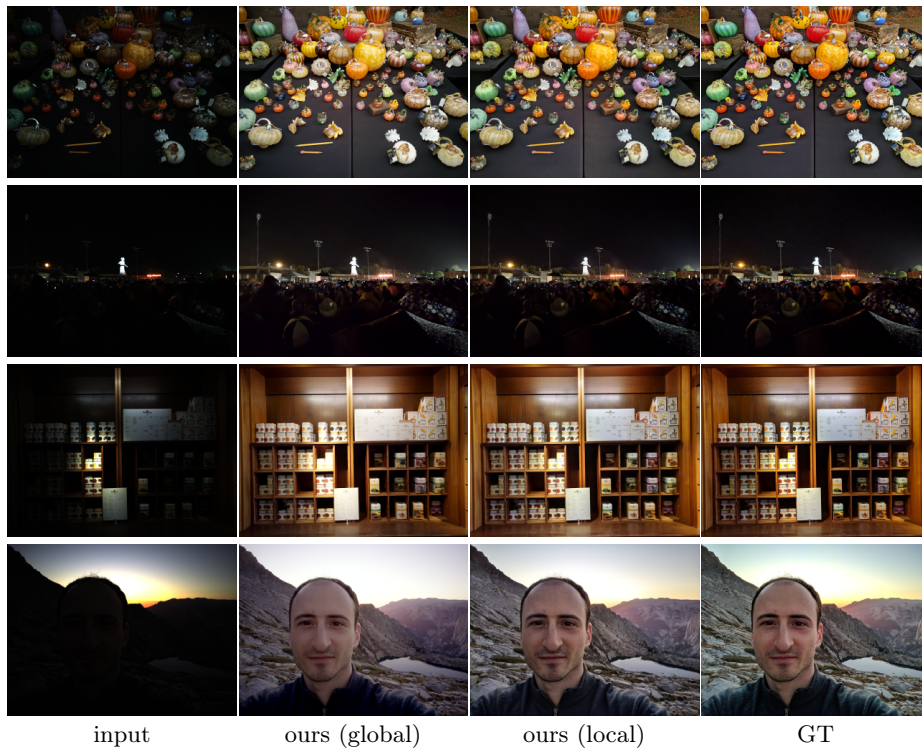


Fig. 9: Visual comparisons of our local and global control on HDR+ dataset [23]. We select bright, dark, and two HDR scenes. In HDR scenes, our local control works better.

References

1. NVIDIA TensorRT. <https://developer.nvidia.com/tensorrt>, [Online; accessed 10-February-2024] **4.3, D**
2. ONNX Runtime. <https://onnxruntime.ai/>, [Online; accessed 10-February-2024] **2.2**
3. TensorFlow Lite. <https://www.tensorflow.org/lite>, [Online; accessed 10-February-2024] **2.2**
4. Affi, M., Barron, J.T., LeGendre, C., Tsai, Y.T., Bleibel, F.: Cross-camera convolutional color constancy. In: Proceedings of the IEEE/CVF International Conference on Computer Vision. pp. 1981–1990 (2021) **2.1**
5. Buades, A., Coll, B., Morel, J.M.: A non-local algorithm for image denoising. In: 2005 IEEE computer society conference on computer vision and pattern recognition (CVPR'05). vol. 2, pp. 60–65. Ieee (2005) **2.1**
6. Bychkovsky, V., Paris, S., Chan, E., Durand, F.: Learning photographic global tonal adjustment with a database of input/output image pairs. In: CVPR 2011. pp. 97–104. IEEE (2011) **1, 4.1, 5, 4, E, 7**
7. Cai, Y., Bian, H., Lin, J., Wang, H., Timofte, R., Zhang, Y.: Retinexformer: One-stage retinex-based transformer for low-light image enhancement. In: Proceedings of the IEEE/CVF International Conference on Computer Vision (ICCV). pp. 12504–12513 (October 2023) **1, 4.3**
8. Chen, L., Chu, X., Zhang, X., Sun, J.: Simple baselines for image restoration. In: European Conference on Computer Vision. pp. 17–33. Springer (2022) **1, 4.3, 2, 5**
9. Chen, Y.S., Wang, Y.C., Kao, M.H., Chuang, Y.Y.: Deep photo enhancer: Unpaired learning for image enhancement from photographs with gans. In: Proceedings of the IEEE conference on computer vision and pattern recognition. pp. 6306–6314 (2018) **4.1**
10. Cheng, D., Prasad, D.K., Brown, M.S.: Illuminant estimation for color constancy: why spatial-domain methods work and the role of the color distribution. *JOSA A* **31**(5), 1049–1058 (2014) **2.1**
11. Conde, M.V., McDonagh, S., Maggioni, M., Leonardis, A., Pérez-Pellitero, E.: Model-based image signal processors via learnable dictionaries. In: Proceedings of the AAAI Conference on Artificial Intelligence. vol. 36, pp. 481–489 (2022) **2.2**
12. Conde, M.V., Vazquez-Corral, J., Brown, M.S., Timofte, R.: Nilut: Conditional neural implicit 3d lookup tables for image enhancement. arXiv preprint arXiv:2306.11920 (2023) **2.2**
13. Dabov, K., Foi, A., Katkounnik, V., Egiazarian, K.: Image denoising by sparse 3-d transform-domain collaborative filtering. *IEEE Transactions on image processing* **16**(8), 2080–2095 (2007) **2.1**
14. Dai, L., Liu, X., Li, C., Chen, J.: Awnet: Attentive wavelet network for image isp. In: Computer Vision–ECCV 2020 Workshops: Glasgow, UK, August 23–28, 2020, Proceedings, Part III 16. pp. 185–201. Springer (2020) **1, 2.1**
15. Dinh, K.Q., Choi, K.P.: End-to-end single-frame image signal processing for high dynamic range scenes. In: Proceedings of the IEEE/CVF Winter Conference on Applications of Computer Vision. pp. 2449–2458 (2023) **2.2**
16. Drago, F., Myszkowski, K., Annen, T., Chiba, N.: Adaptive logarithmic mapping for displaying high contrast scenes. In: Computer graphics forum. vol. 22, pp. 419–426. Wiley Online Library (2003) **2.1**
17. Ershov, E., Savchik, A., Shepelev, D., Banić, N., Brown, M.S., Timofte, R., Koščević, K., Freeman, M., Tesalin, V., Bocharov, D., et al.: Ntire 2022 challenge on

- night photography rendering. In: Proceedings of the IEEE/CVF Conference on Computer Vision and Pattern Recognition. pp. 1287–1300 (2022) [2.1](#)
18. Ershov, E., Tesalin, V., Ermakov, I., Brown, M.S.: Physically-plausible illumination distribution estimation. In: Proceedings of the IEEE/CVF International Conference on Computer Vision. pp. 12928–12936 (2023) [2.1](#)
 19. Gharbi, M., Chen, J., Barron, J.T., Hasinoff, S.W., Durand, F.: Deep bilateral learning for real-time image enhancement. *ACM Transactions on Graphics (TOG)* **36**(4), 1–12 (2017) [1](#), [2](#)
 20. Gou, W., Yi, Z., Xiang, Y., Li, S., Liu, Z., Kong, D., Xu, K.: Syenet: A simple yet effective network for multiple low-level vision tasks with real-time performance on mobile device. In: Proceedings of the IEEE/CVF International Conference on Computer Vision. pp. 12182–12195 (2023) [1](#), [2.1](#), [3.2](#), [3](#), [1](#), [2](#), [3](#), [5](#)
 21. Gu, B., Li, W., Zhu, M., Wang, M.: Local edge-preserving multiscale decomposition for high dynamic range image tone mapping. *IEEE Transactions on Image Processing* **22**(1), 70–79 (2012) [2.1](#), [2.2](#)
 22. Hansen, P., Vilkin, A., Krustalev, Y., Imber, J., Talagala, D., Hanwell, D., Mattina, M., Whatmough, P.N.: Isp4ml: The role of image signal processing in efficient deep learning vision systems. In: 2020 25th International Conference on Pattern Recognition (ICPR). pp. 2438–2445. IEEE (2021) [1](#)
 23. Hasinoff, S.W., Sharlet, D., Geiss, R., Adams, A., Barron, J.T., Kainz, F., Chen, J., Levoy, M.: Burst photography for high dynamic range and low-light imaging on mobile cameras. *ACM Transactions on Graphics (Proc. SIGGRAPH Asia)* **35**(6) (2016) [4.1](#), [9](#)
 24. He, J., Liu, Y., Qiao, Y., Dong, C.: Conditional sequential modulation for efficient global image retouching. In: Computer Vision–ECCV 2020: 16th European Conference, Glasgow, UK, August 23–28, 2020, Proceedings, Part XIII 16. pp. 679–695. Springer (2020) [1](#), [2](#)
 25. Hevia, L.V., Patricio, M.A., Molina, J.M., Berlanga, A.: Optimization of the isp parameters of a camera through differential evolution. *IEEE Access* **8**, 143479–143493 (2020) [2.1](#)
 26. Ignatov, A., Chiang, C.M., Kuo, H.K., Sycheva, A., Timofte, R.: Learned smartphone isp on mobile npus with deep learning, mobile ai 2021 challenge: Report. In: Proceedings of the IEEE/CVF Conference on Computer Vision and Pattern Recognition. pp. 2503–2514 (2021) [4.1](#), [8](#)
 27. Ignatov, A., Sycheva, A., Timofte, R., Tseng, Y., Xu, Y.S., Yu, P.H., Chiang, C.M., Kuo, H.K., Chen, M.H., Cheng, C.M., et al.: Microisp: processing 32mp photos on mobile devices with deep learning. In: European Conference on Computer Vision. pp. 729–746. Springer (2022) [1](#), [2.1](#), [1](#), [4.3](#), [3](#), [5](#)
 28. Ignatov, A., Timofte, R., Liu, S., Feng, C., Bai, F., Wang, X., Lei, L., Yi, Z., Xiang, Y., Liu, Z., et al.: Learned smartphone isp on mobile gpus with deep learning, mobile ai & aim 2022 challenge: report. In: European Conference on Computer Vision. pp. 44–70. Springer (2022) [4.1](#), [3](#)
 29. Ignatov, A., Van Gool, L., Timofte, R.: Replacing mobile camera isp with a single deep learning model. In: Proceedings of the IEEE/CVF Conference on Computer Vision and Pattern Recognition Workshops. pp. 536–537 (2020) [1](#), [2.1](#)
 30. Johnson, J., Alahi, A., Fei-Fei, L.: Perceptual losses for real-time style transfer and super-resolution. In: Computer Vision–ECCV 2016: 14th European Conference, Amsterdam, The Netherlands, October 11–14, 2016, Proceedings, Part II 14. pp. 694–711. Springer (2016) [4.2](#)

31. Li, J., Zhang, Z., Liu, X., Feng, C., Wang, X., Lei, L., Zuo, W.: Spatially adaptive self-supervised learning for real-world image denoising. In: Proceedings of the IEEE/CVF Conference on Computer Vision and Pattern Recognition. pp. 9914–9924 (2023) [2.1](#)
32. Liang, Z., Cai, J., Cao, Z., Zhang, L.: Cameranet: A two-stage framework for effective camera isp learning. *IEEE Transactions on Image Processing* **30**, 2248–2262 (2021) [2.1](#)
33. Liu, S., Feng, C., Wang, X., Wang, H., Zhu, R., Li, Y., Lei, L.: Deep-flexisp: A three-stage framework for night photography rendering. In: Proceedings of the IEEE/CVF Conference on Computer Vision and Pattern Recognition. pp. 1211–1220 (2022) [2.1](#)
34. Liu, W., Li, W., Zhu, J., Cui, M., Xie, X., Zhang, L.: Improving nighttime driving-scene segmentation via dual image-adaptive learnable filters. *IEEE Transactions on Circuits and Systems for Video Technology* (2023) [1](#)
35. Loshchilov, I., Hutter, F.: Sgdr: Stochastic gradient descent with warm restarts. arXiv preprint arXiv:1608.03983 (2016) [4.2](#)
36. Loshchilov, I., Hutter, F.: Decoupled weight decay regularization. arXiv preprint arXiv:1711.05101 (2017) [4.2](#)
37. Moran, S., Marza, P., McDonagh, S., Parisot, S., Slabaugh, G.: Deeplpf: Deep local parametric filters for image enhancement. In: Proceedings of the IEEE/CVF conference on computer vision and pattern recognition. pp. 12826–12835 (2020) [2](#)
38. Mosleh, A., Sharma, A., Onzon, E., Mannan, F., Robidoux, N., Heide, F.: Hardware-in-the-loop end-to-end optimization of camera image processing pipelines. In: Proceedings of the IEEE/CVF Conference on Computer Vision and Pattern Recognition. pp. 7529–7538 (2020) [1](#), [2.1](#), [3.1](#)
39. Onzon, E., Mannan, F., Heide, F.: Neural auto-exposure for high-dynamic range object detection. In: Proceedings of the IEEE/CVF Conference on Computer Vision and Pattern Recognition. pp. 7710–7720 (2021) [2.1](#)
40. Otsuka, J., Yoshimura, M., Ohashi, T.: Self-supervised reversed image signal processing via reference-guided dynamic parameter selection. arXiv preprint arXiv:2303.13916 (2023) [2.2](#)
41. Ouyang, W., Dong, Y., Kang, X., Ren, P., Xu, X., Xie, X.: Rsfnet: A white-box image retouching approach using region-specific color filters. In: Proceedings of the IEEE/CVF International Conference on Computer Vision. pp. 12160–12169 (2023) [1](#)
42. Paszke, A., Gross, S., Massa, F., Lerer, A., Bradbury, J., Chanan, G., Killeen, T., Lin, Z., Gimelshein, N., Antiga, L., et al.: Pytorch: An imperative style, high-performance deep learning library. *Advances in neural information processing systems* **32** (2019) [4.3](#), [D](#)
43. Pavithra, G., Radhesh, B.: Automatic image quality tuning framework for optimization of isp parameters based on multi-stage optimization approach. *Electronic Imaging* **2021**(9), 197–1 (2021) [2.1](#)
44. Punnappurath, A., Abuolaim, A., Abdelhamed, A., Levinshtein, A., Brown, M.S.: Day-to-night image synthesis for training nighttime neural isps. In: Proceedings of the IEEE/CVF Conference on Computer Vision and Pattern Recognition. pp. 10769–10778 (2022) [1](#)
45. Qin, H., Han, L., Wang, J., Zhang, C., Li, Y., Li, B., Hu, W.: Attention-aware learning for hyperparameter prediction in image processing pipelines. In: European Conference on Computer Vision. pp. 271–287. Springer (2022) [1](#), [2.2](#)

46. Qin, H., Han, L., Xiong, W., Wang, J., Ma, W., Li, B., Hu, W.: Learning to exploit the sequence-specific prior knowledge for image processing pipelines optimization. In: Proceedings of the IEEE/CVF Conference on Computer Vision and Pattern Recognition. pp. 22314–22323 (2023) [1](#), [2.2](#)
47. Rombach, R., Blattmann, A., Lorenz, D., Esser, P., Ommer, B.: High-resolution image synthesis with latent diffusion models. In: Proceedings of the IEEE/CVF conference on computer vision and pattern recognition. pp. 10684–10695 (2022) [3.3](#)
48. Ronneberger, O., Fischer, P., Brox, T.: U-net: Convolutional networks for biomedical image segmentation. In: Medical Image Computing and Computer-Assisted Intervention–MICCAI 2015: 18th International Conference, Munich, Germany, October 5–9, 2015, Proceedings, Part III 18. pp. 234–241. Springer (2015) [B](#)
49. Shen, H., Zhao, Z.Q., Zhang, W.: Adaptive dynamic filtering network for image denoising. In: Proceedings of the AAAI Conference on Artificial Intelligence. vol. 37, pp. 2227–2235 (2023) [3.1](#)
50. Shi, W., Caballero, J., Huszár, F., Totz, J., Aitken, A.P., Bishop, R., Rueckert, D., Wang, Z.: Real-time single image and video super-resolution using an efficient sub-pixel convolutional neural network. In: Proceedings of the IEEE conference on computer vision and pattern recognition. pp. 1874–1883 (2016) [B](#)
51. Shibata, T., Tanaka, M., Okutomi, M.: Gradient-domain image reconstruction framework with intensity-range and base-structure constraints. In: Proceedings of the IEEE conference on computer vision and pattern recognition. pp. 2745–2753 (2016) [2.1](#), [2.2](#)
52. Shutova, A., Ershov, E., Perevozchikov, G., Ermakov, I., Banić, N., Timofte, R., Collins, R., Efimova, M., Terekhin, A., Zini, S., et al.: Ntire 2023 challenge on night photography rendering. In: Proceedings of the IEEE/CVF Conference on Computer Vision and Pattern Recognition. pp. 1981–1992 (2023) [2.1](#)
53. Simonyan, K., Zisserman, A.: Very deep convolutional networks for large-scale image recognition. arXiv preprint arXiv:1409.1556 (2014) [4.2](#)
54. Stevens, S.S.: On the psychophysical law. *Psychological review* **64**(3), 153–181 (1957) [1](#)
55. Tseng, E., Yu, F., Yang, Y., Mannan, F., Arnaud, K.S., Nowrouzezahrai, D., Lalonde, J.F., Heide, F.: Hyperparameter optimization in black-box image processing using differentiable proxies. *ACM Trans. Graph.* **38**(4), 27–1 (2019) [1](#), [3.4](#)
56. Van De Weijer, J., Gevers, T., Gijsenij, A.: Edge-based color constancy. *IEEE Transactions on image processing* **16**(9), 2207–2214 (2007) [2.1](#)
57. Wang, R., Zhang, Q., Fu, C.W., Shen, X., Zheng, W.S., Jia, J.: Underexposed photo enhancement using deep illumination estimation. In: Proceedings of the IEEE/CVF conference on computer vision and pattern recognition. pp. 6849–6857 (2019) [1](#)
58. Wu, C.T., Isikdogan, L.F., Rao, S., Nayak, B., Gerasimow, T., Sutic, A., Ainkedem, L., Michael, G.: Visionisp: Repurposing the image signal processor for computer vision applications. In: 2019 IEEE International Conference on Image Processing (ICIP). pp. 4624–4628. IEEE (2019) [2.1](#)
59. Yang, C., Jin, M., Jia, X., Xu, Y., Chen, Y.: Adaint: Learning adaptive intervals for 3d lookup tables on real-time image enhancement. In: Proceedings of the IEEE/CVF Conference on Computer Vision and Pattern Recognition. pp. 17522–17531 (2022) [2.1](#), [2.2](#), [1](#), [4.3](#), [A](#)

60. Yang, C., Jin, M., Xu, Y., Zhang, R., Chen, Y., Liu, H.: Seplut: Separable image-adaptive lookup tables for real-time image enhancement. In: European Conference on Computer Vision. pp. 201–217. Springer (2022) [2.1](#), [2.2](#), [4.1](#), [1](#), [4.3](#), [4.5](#), [A](#), [5](#), [D](#)
61. Yoshimura, M., Otsuka, J., Irie, A., Ohashi, T.: Dynamicisp: dynamically controlled image signal processor for image recognition. In: Proceedings of the IEEE/CVF International Conference on Computer Vision. pp. 12866–12876 (2023) [1](#), [2.2](#), [3](#), [3.1](#), [2](#)
62. Yoshimura, M., Otsuka, J., Irie, A., Ohashi, T.: Rawgment: noise-accounted raw augmentation enables recognition in a wide variety of environments. In: Proceedings of the IEEE/CVF Conference on Computer Vision and Pattern Recognition. pp. 14007–14017 (2023) [1](#), [2.1](#), [3.1](#)
63. Zamir, S.W., Arora, A., Khan, S., Hayat, M., Khan, F.S., Yang, M.H.: Restormer: Efficient transformer for high-resolution image restoration. In: Proceedings of the IEEE/CVF conference on computer vision and pattern recognition. pp. 5728–5739 (2022) [1](#)
64. Zeng, H., Cai, J., Li, L., Cao, Z., Zhang, L.: Learning image-adaptive 3d lookup tables for high performance photo enhancement in real-time. IEEE Transactions on Pattern Analysis and Machine Intelligence **44**(4), 2058–2073 (2020) [2.2](#), [4.1](#), [1](#), [4.3](#), [2](#), [4.5](#), [A](#)
65. Zhang, F., Tian, M., Li, Z., Xu, B., Lu, Q., Gao, C., Sang, N.: Lookup table meets local laplacian filter: Pyramid reconstruction network for tone mapping. Advances in Neural Information Processing Systems **36** (2024) [4.1](#), [1](#), [4.3](#), [2](#), [A](#)
66. Zhang, F., Zeng, H., Zhang, T., Zhang, L.: Clut-net: Learning adaptively compressed representations of 3dluts for lightweight image enhancement. In: Proceedings of the 30th ACM International Conference on Multimedia. pp. 6493–6501 (2022) [2](#)
67. Zhang, Z., Wang, H., Liu, M., Wang, R., Zhang, J., Zuo, W.: Learning raw-to-srgb mappings with inaccurately aligned supervision. In: Proceedings of the IEEE/CVF International Conference on Computer Vision. pp. 4348–4358 (2021) [2.1](#)
68. Zhou, J., Jampani, V., Pi, Z., Liu, Q., Yang, M.H.: Decoupled dynamic filter networks. In: Proceedings of the IEEE/CVF Conference on Computer Vision and Pattern Recognition. pp. 6647–6656 (2021) [3.1](#), [4.5](#)
69. Zini, S., Rota, C., Buzzelli, M., Bianco, S., Schettini, R.: Back to the future: a night photography rendering isp without deep learning. In: Proceedings of the IEEE/CVF Conference on Computer Vision and Pattern Recognition. pp. 1465–1473 (2023) [2.1](#)
70. Zou, Y., Yan, C., Fu, Y.: Iterative denoiser and noise estimator for self-supervised image denoising. In: Proceedings of the IEEE/CVF International Conference on Computer Vision. pp. 13265–13274 (2023) [2.1](#)